CHAPTER 5
SPECTRAL FIT ALGORITHM

The Gaussian Transformation algorithm presented in Chapter 4 failed because it made an assumption about the transmitted spectrum that was not accurate. Hence, the second algorithm involved solving for both the total attenuation and the scatterer size using a single minimization routine to fit a curve to the backscattered spectrum without making any assumptions about the form of the scattered spectrum and was termed the Spectral Fit algorithm. In this chapter, the Spectral Fit algorithm will be introduced and several modifications to the algorithm will be discussed.

5.1 Basic Spectral Fit Algorithm

Initially, the Spectral Fit algorithm was implemented using many of the same processing techniques introduced in the Gaussian Transformation algorithm. Weakly focused transducers, "small" window lengths, and a linear frequency dependence of the attenuation along the propagation path were assumed, so that A_{comp} could be approximated as $e^{4z_T\alpha_o f}$. Then, P_{scat} was found by averaging the spectra from 25 independent RF echoes in the log domain according to Equation (4.6), and the effects of electronic noise were reduced by dividing by $\left(1+E_N\left[\left|N(f)\right|^2\right]\Big/P_{scat}(f)\Big|_{measured}\right)$ as was described in Chapter 4. Hence,

$$P_{scat}(f)=\frac{\exp\left(\frac{1}{25}\sum_{i=1}^{25}\ln\left(\left|V_i\right|^2\right)\right)}{\left(1+E_N\left[\left|N(f)\right|^2\right]\Big/\exp\left(\frac{1}{25}\sum_{i=1}^{25}\ln\left(\left|V_i\right|^2\right)\right)\right)} \tag{5.1}$$

in the first implementation of the algorithm. Also, the echo signal from a rigid plane positioned at the focus was simulated, windowed by the same hamming window used to window the simulated backscattered signal, and multiplied by k_o^4 yielding

$$P_{ref}(f) = k_o^4 \left|V_{inc}(\omega)\right|^2 \left|H(\omega)\right|^4 \propto k_o^4 \left|V_{plane}(\omega)\right|^2. \tag{5.2}$$

The scatterer size and total attenuation along the propagation path were then found by finding the values of a_{eff} and α_o that minimized the error given by

$$ASD = \underset{f}{\text{mean}}\left[\left(X\left(f, a_{eff}, \alpha_o\right) - \overline{X}\left(a_{eff}, \alpha_o\right)\right)^2\right], \tag{5.3}$$

where

$$X\left(f, a_{eff}, \alpha_o\right) = \ln\left(\frac{P_{scat}(f)}{\max_f\left(P_{scat}(f)\right)}\right) - \ln\left(\frac{P_{ref}(f)F\left(f, a_{eff}\right)e^{-4\alpha_o f z_T}}{\max_f\left(P_{ref}(f)F\left(f, a_{eff}\right)e^{-4\alpha_o f z_T}\right)}\right) \tag{5.4}$$

$$\overline{X}\left(a_{eff}, \alpha_o\right) = \underset{f}{\text{mean}}\left[X\left(f, a_{eff}, \alpha_o\right)\right].$$

Also, the range of frequencies initially selected for the minimization in this algorithm was given by Equation (4.9) for the initial simulations.

5.1.1 Initial simulation results

The performance of the Spectral Fit algorithm was also evaluated by computer simulations designed to test its performance with increasing attenuation and electronic noise. The same simulated scattered signals described in Chapter 4 for the Gaussian Transformation simulations were also used to perform the initial evaluation of this algorithm. Hence, 40 independent estimates of scatterer size and attenuation were found for half-spaces with attentions between 0 and 1 dB/cm/MHz. The results for an attenuation of 0.3 dB/cm/MHz for all of the attempted hamming window lengths in the absence of any electronic noise are shown in Figure 5.1. The error bars are the same as those defined by Equations (4.18) and (4.19). For large window lengths, the algorithm provides a reasonable estimate for scatterer size and total attenuation. However, as the window length is decreased, both the precision and accuracy of the estimates degrade. The loss of accuracy is due to the convolution effects of the windowing function [*Akita and Ueda*, 1988]. Likewise, the loss of precision at smaller window lengths is probably due to a reduction in the number of independent samples in the least squares fit in Equation (5.3) due to a loss in the frequency resolution of the spectrum [*Wear*, 2001b].

The degradation with window length was also observed in other values of attenuation as is summarized in Figure 5.2. These plots also show that the precision of the attenuation estimate as well as the precision and accuracy of the scatterer size estimate degrade with increasing

attenuation. However, consistently reasonable estimates with errors in scatterer size less than 20% are still obtainable for attenuations as high as 0.6 dB/cm/MHz at a window length of 8 mm.

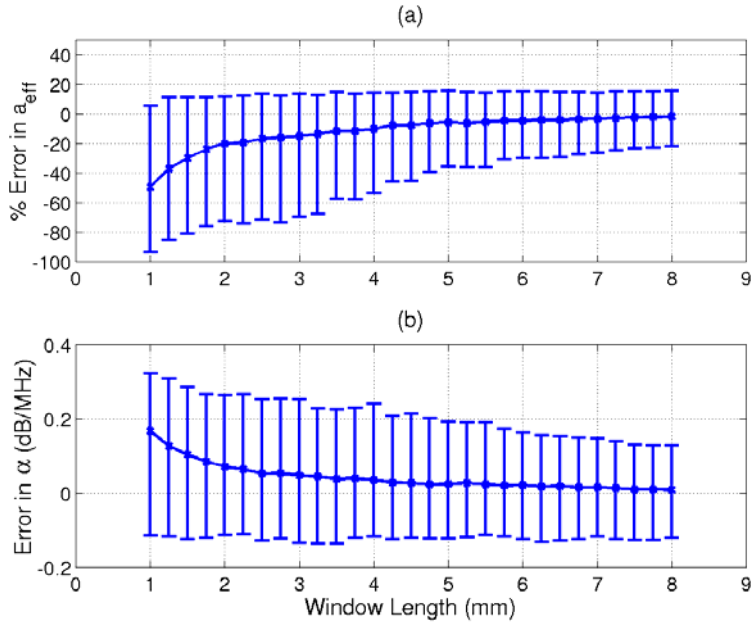

Figure 5.1: Errors in estimated (a) scatterer size and (b) total attenuation for different hamming window lengths for an attenuation of 0.3 dB/cm/MHz in the absence of any electronic noise.

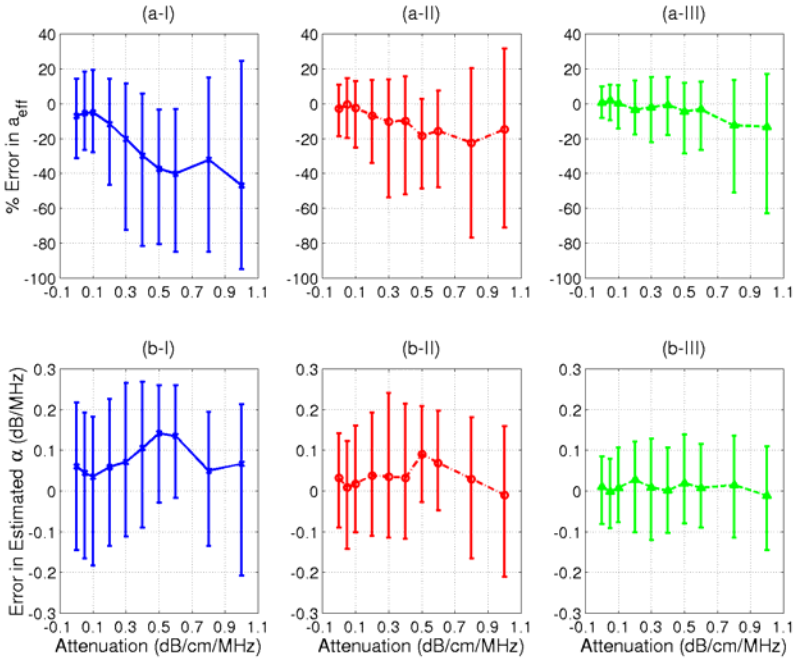

Figure 5.2: Plot of errors in estimated (a) scatterer size and (b) total attenuation for different values of attenuation with hamming window lengths of (I) 2 mm, (II) 4 mm, and (III) 8 mm in the absence of any electronic noise.

The effect of electronic noise was also evaluated by adding white Gaussian noise of varying powers to the simulated RF echoes in the time domain. For each noise level and for half-space attenuations between 0.05 and 1 dB/cm/MHz, the scatterer size and total attenuation were estimated. The results of these simulations are shown in Figures 5.3 through 5.11. The reported *SNR* shown in each figure was calculated using Equation (4.20). The algorithm gives reasonably accurate average estimates of the scatterer size with errors less than 20% down to *SNR*s of 6 dB for all of the different values of half-space attenuation and window lengths of 4 mm and 8 mm. Likewise, the average estimate for the total attenuation had errors of less than 0.2 dB/MHz for all of the tested *SNR*s. This translates to an error of about 20% when estimating the amplitude of the pressure field at 8 MHz in the focal region. Unfortunately, the algorithm is not very precise as can be seen from the large error bars about the average values. As a result, consistently precise estimates (errors <20%) can only be obtained for *SNR*s better than 23 dB for half-space attenuations between 0.05-0.3 dB/cm/MHz and better than 28 dB for half-space attenuations between 0.4-0.6 dB/cm/MHz for the window length of 8 mm. The performance of the 4 mm window lengths is even worse. Improving the precision to allow for smaller *SNR*s, higher attenuations, and smaller window lengths was the focus of the rest of this investigation.

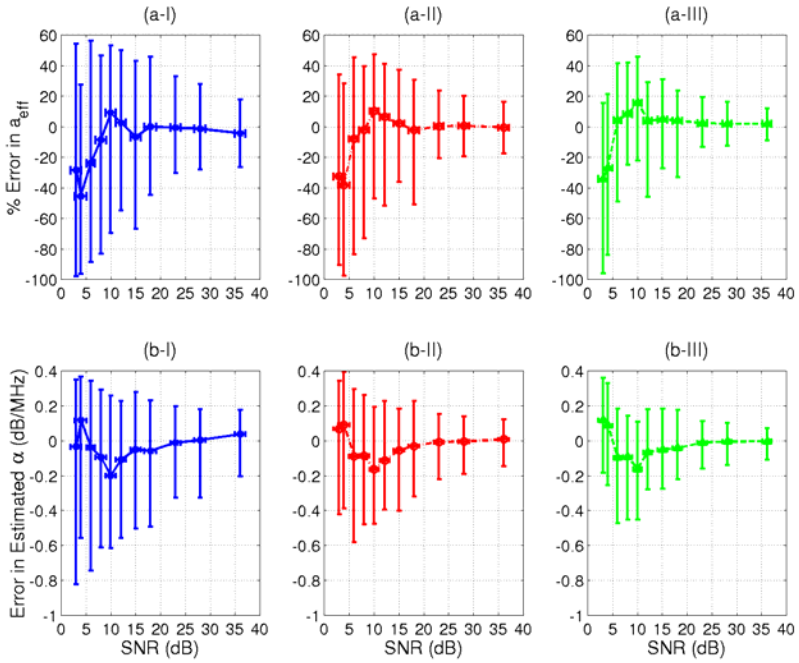

Figure 5.3: Errors in estimates of (a) scatterer size and (b) total attenuation for different levels of electronic noise for a half-space attenuation of 0.05 dB/cm/MHz and hamming window lengths of (I) 2 mm, (II) 4 mm, and (III) 8 mm.

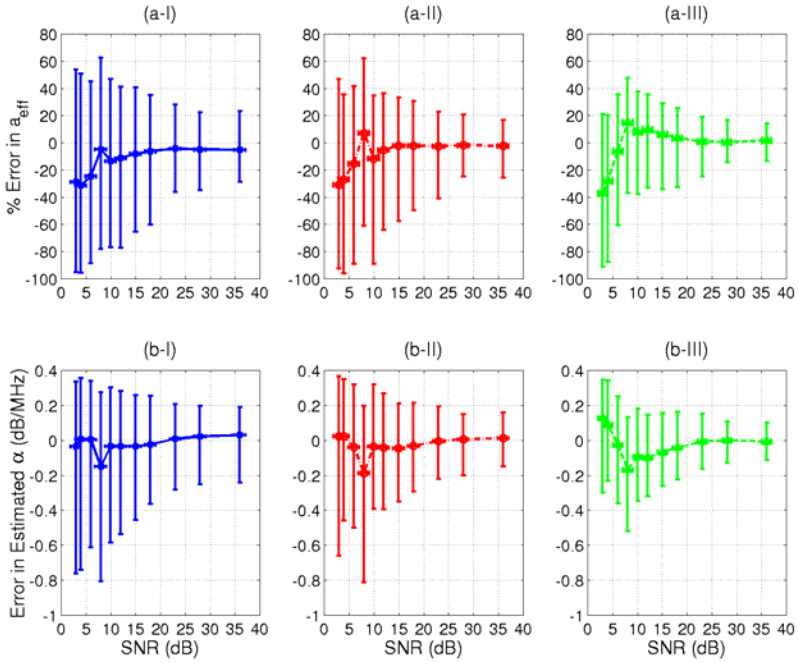

Figure 5.4: Errors in estimates of (a) scatterer size and (b) total attenuation for different levels of electronic noise for a half-space attenuation of 0.1 dB/cm/MHz and hamming window lengths of (I) 2 mm, (II) 4 mm, and (III) 8 mm.

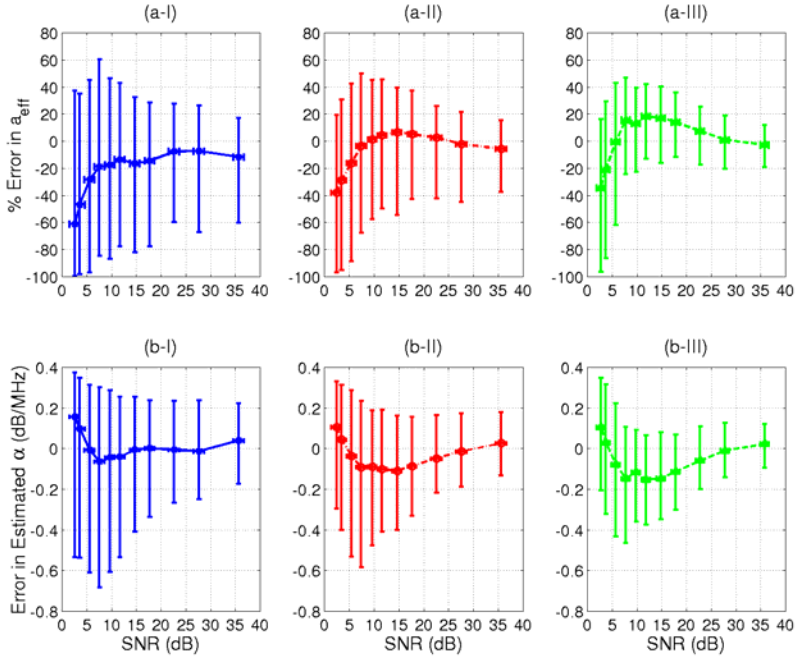

Figure 5.5: Errors in estimates of (a) scatterer size and (b) total attenuation for different levels of electronic noise for a half-space attenuation of 0.2 dB/cm/MHz and hamming window lengths of (I) 2 mm, (II) 4 mm, and (III) 8 mm.

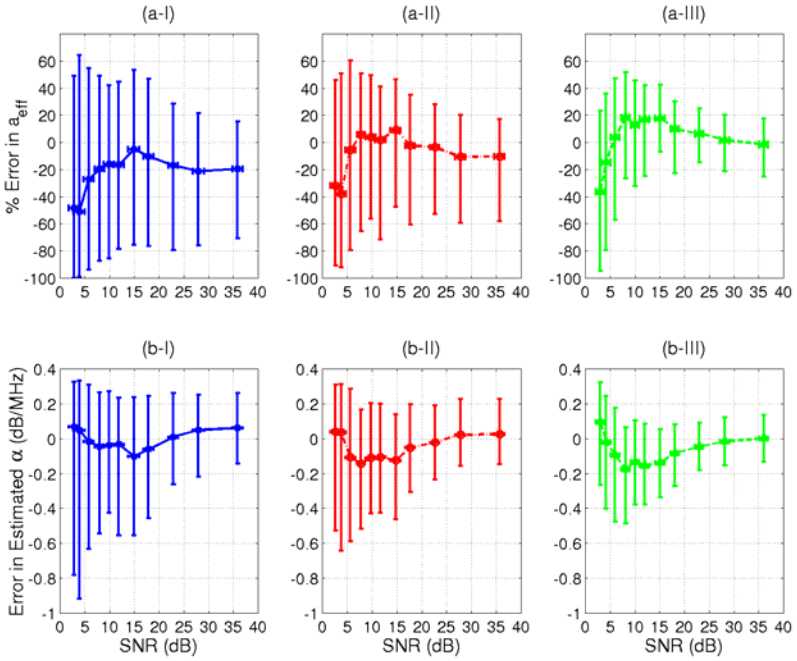

Figure 5.6: Errors in estimates of (a) scatterer size and (b) total attenuation for different levels of electronic noise for a half-space attenuation of 0.3 dB/cm/MHz and hamming window lengths of (I) 2 mm, (II) 4 mm, and (III) 8 mm.

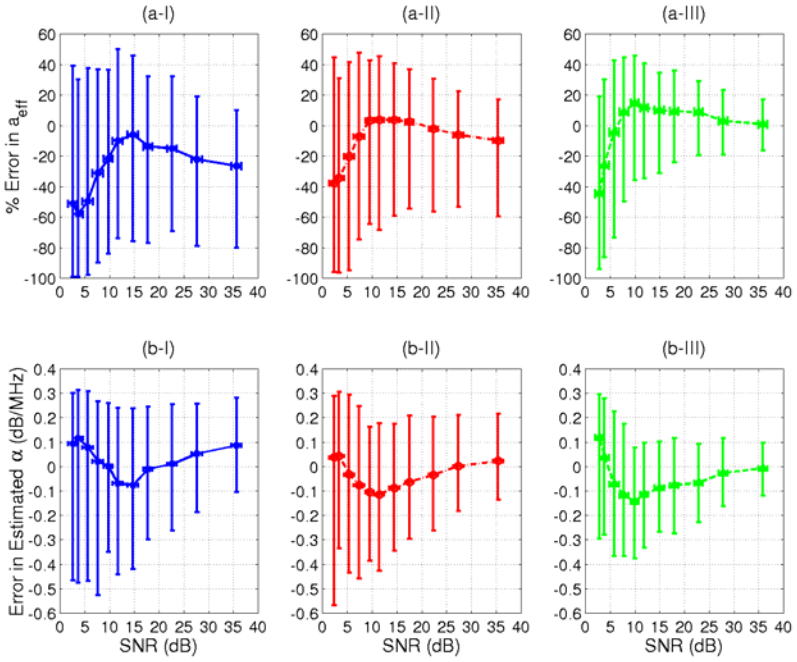

Figure 5.7: Errors in estimates of (a) scatterer size and (b) total attenuation for different levels of electronic noise for a half-space attenuation of 0.4 dB/cm/MHz and hamming window lengths of (I) 2 mm, (II) 4 mm, and (III) 8 mm.

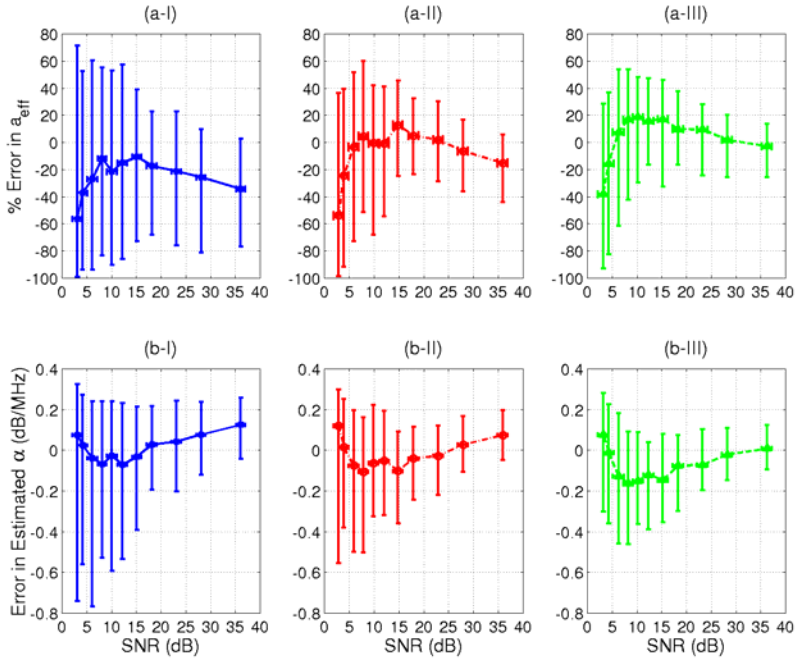

Figure 5.8: Errors in estimates of (a) scatterer size and (b) total attenuation for different levels of electronic noise for a half-space attenuation of 0.5 dB/cm/MHz and hamming window lengths of (I) 2 mm, (II) 4 mm, and (III) 8 mm.

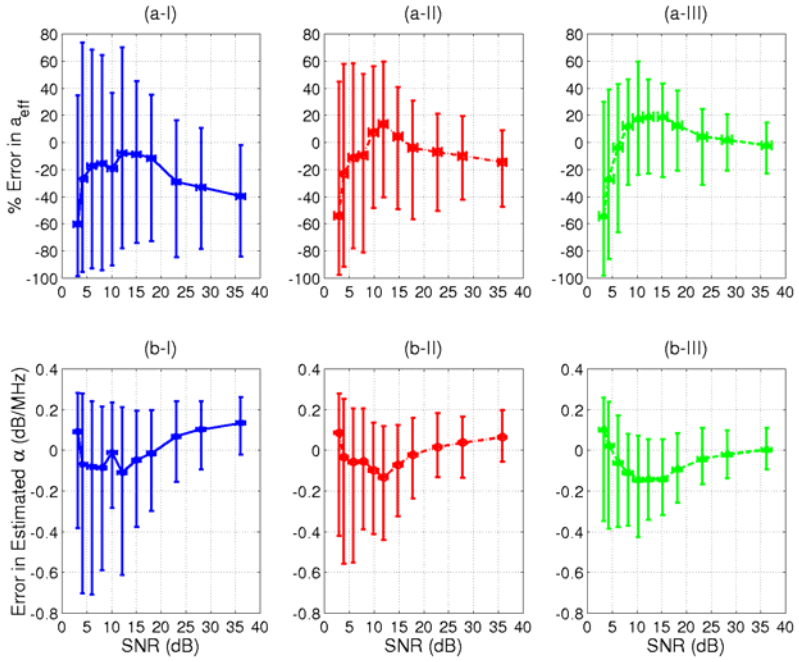

Figure 5.9: Errors in estimates of (a) scatterer size and (b) total attenuation for different levels of electronic noise for a half-space attenuation of 0.6 dB/cm/MHz and hamming window lengths of (I) 2 mm, (II) 4 mm, and (III) 8 mm.

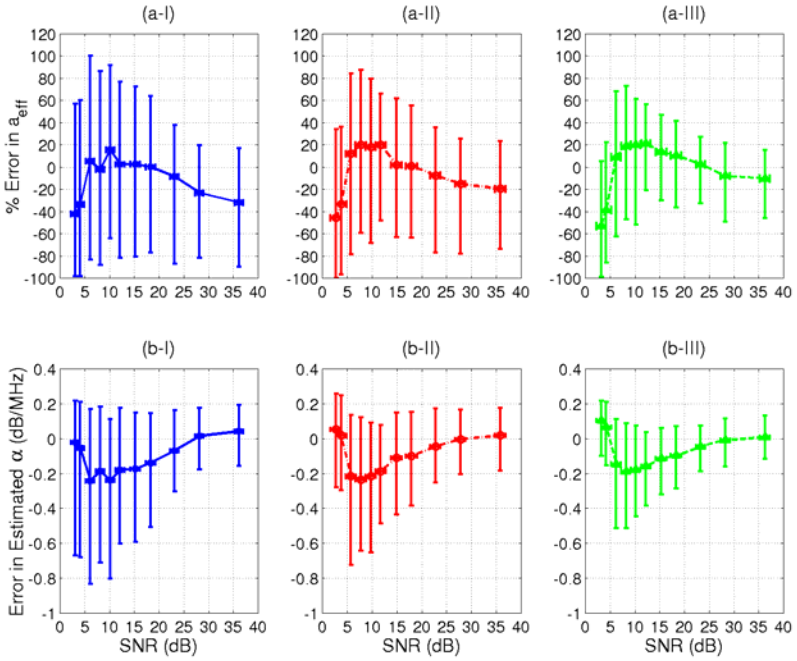

Figure 5.10: Errors in estimates of (a) scatterer size and (b) total attenuation for different levels of electronic noise for a half-space attenuation of 0.8 dB/cm/MHz and hamming window lengths of (I) 2 mm, (II) 4 mm, and (III) 8 mm.

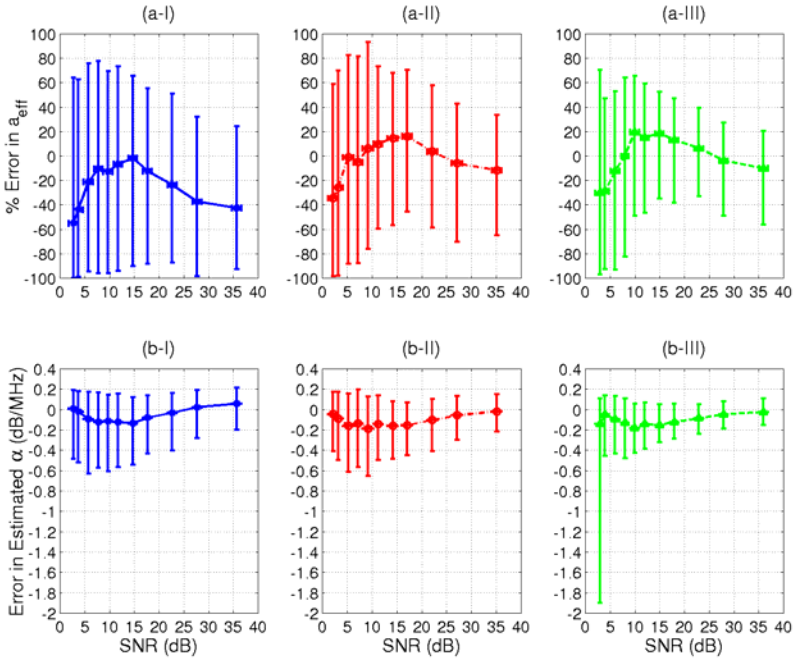

Figure 5.11: Errors in estimates of (a) scatterer size and (b) total attenuation for different levels of electronic noise for a half-space attenuation of 1 dB/cm/MHz and hamming window lengths of (I) 2 mm, (II) 4 mm, and (III) 8 mm.

5.2 Modifications to the Basic Spectral Fit Algorithm

While the Spectral Fit algorithm was being tested, some of the processing steps were evaluated and improved. Hence, before concluding this chapter, several modifications to the algorithm need to be discussed.

5.2.1 Noise reduction techniques

The first processing steps evaluated involved those associated with reducing the noise before performing the estimate. First, recall from Chapter 4 that the spectral noise resulting from the random scatterer spacing was reduced by averaging the spectra of the 25 pulse-echo waveforms in the log domain as given by Equation (4.6). Traditionally, however, the averaging of the spectra is done in the regular frequency domain [*Insana et al.*, 1990] or

$$P_{scat}(f) = \frac{1}{25}\sum_{j=1}^{25}\left|V_j\right|^2 . \tag{5.5}$$

A comparison of the two averaging methods is provided in Figure 5.12 for a half-space attenuation of 0.3 dB/cm/MHz in the absence of any electronic noise. The mean values of the estimates are almost identical, but the deviation in the estimates, given by adding together the upper and lower error bars, is slightly larger when averaging in the log domain. Hence, one method to reduce the variance in the estimator in future algorithms would be to average in the normal spectral domain rather than the log domain.

The second noise reduction technique evaluated was the division of the averaged spectrum by $\left(1+\mathrm{E}_N\left[\left|N(f)\right|^2\right]\Big/P_{scat}(f)\Big|_{measured}\right)$ to reduce the impact of electronic noise. The evaluation was done by comparing the results for three different levels of electronic noise both with and without the compensating term for a half-space with an attenuation of 0.05 dB/cm/MHz. The errors in the average estimates are shown in Figure 5.13. In this evaluation, the averaging of the 25 spectra was still done in the log domain. From Figure 5.13, it is clear that the electronic noise compensation term $\left(1+\mathrm{E}_N\left[\left|N(f)\right|^2\right]\Big/P_{scat}(f)\Big|_{measured}\right)$ greatly improves the accuracy of the estimates in the presence of electronic system noise.

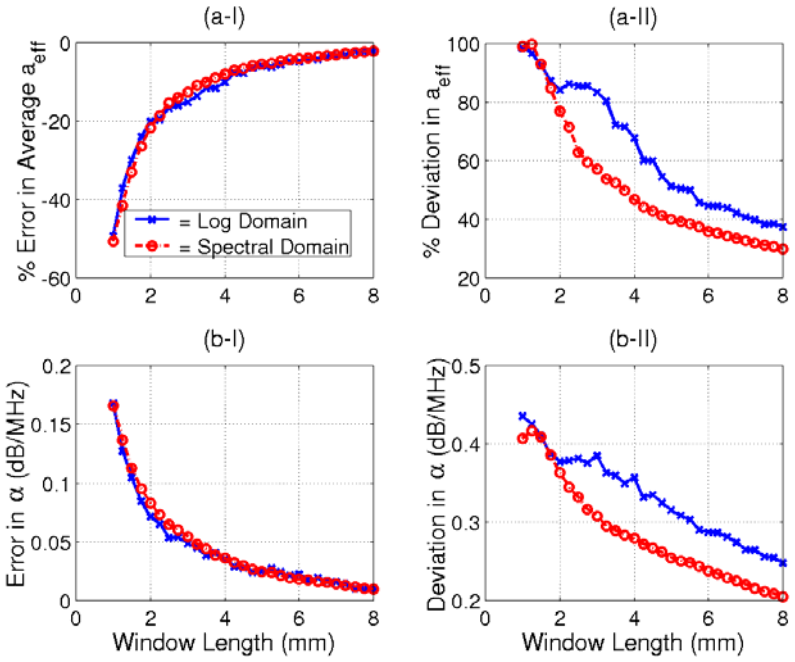

Figure 5.12: A comparison between averaging in the normal spectral domain and the log spectral domain to reduce spectral noise due to random scatterer spacing for a half-space with an attenuation of 0.3 dB/cm/MHz in the absence of any electronic noise. Plots (a) compare the scatterer size estimates and plots (b) compare the total attenuation estimates. Plots (I) show the errors in the mean value for the estimates and plots (II) show the total deviation about the mean estimated values.

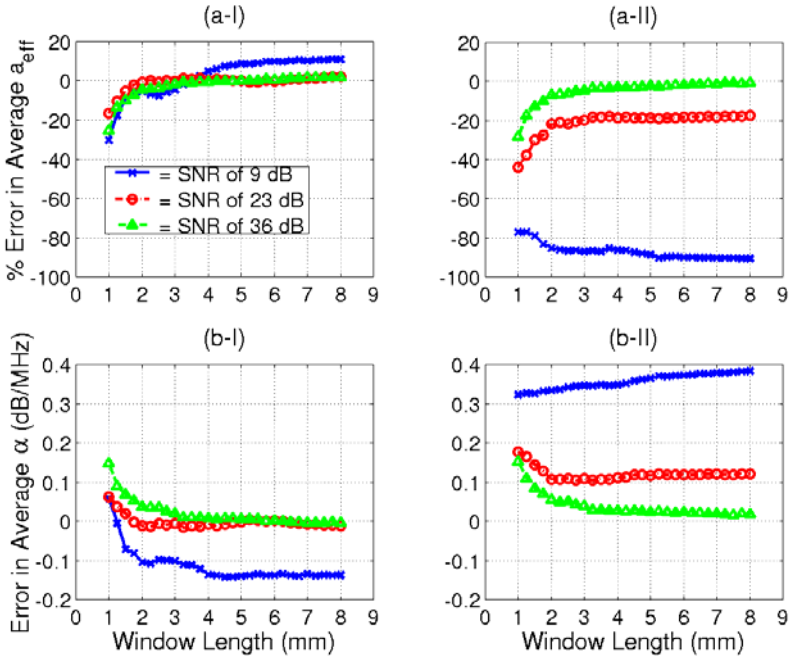

Figure 5.13: Comparison of errors in average estimate of (a) scatterer size and (b) total attenuation both (I) with and (II) without noise compensation for a half-space with an attenuation of 0.05 dB/cm/MHz.

Although tested when averaging in the log domain, the error correction term would still apply when averaging in the normal spectral domain because Equation (4.14) would become

$$P_{scat}(f) = \frac{1}{25}\sum_{i=1}^{25}\left(\left|V_i(f)\right|^2\left(1+\frac{E_N\left[\left|N(f)\right|^2\right]}{\left|V_i(f)\right|^2}\right)\right)$$

$$= \frac{1}{25}\sum_{i=1}^{25}\left|V_i(f)\right|^2 + E_N\left[\left|N(f)\right|^2\right] \tag{5.6}$$

$$= P_{scat}(f)_{ideal}\left(1+\frac{E_N\left[\left|N(f)\right|^2\right]}{P_{scat}(f)_{ideal}}\right).$$

Hence,

$$P_{scat}(f)\big|_{ideal} \cong \frac{P_{scat}(f)\big|_{measured}}{\left(1+\dfrac{E_N\left[\left|N(f)\right|^2\right]}{P_{scat}(f)\big|_{measured}}\right)} \tag{5.7}$$

indicating that dividing by $\left(1+\mathrm{E}_N\left[\left|N(f)\right|^2\right]\Big/P_{scat}(f)\big|_{measured}\right)$ should still decrease the impact of electronic noise. This hypothesis is validated in Section 5.2.3.

5.2.2 Windowing function compensation

In the initial algorithms considered, compensating for the effects of windowing (i.e. blurring of the spectrum) was done by applying the same window of length *L* to both the reference signal and the backscattered signal while accounting for the difference in sound speed. Also, a hamming window was used to perform the windowing. However, it is not clear that this is the best approach. Therefore, in this section, other windowing schemes and compensation methods are considered within the framework of the Spectral Fit algorithm. The algorithm remains the same as discussed in Section 5.1 with the exception that the spectra from adjacent RF echoes are averaged in the regular frequency domain instead of the log frequency domain.

Initially, three different simulations were preformed using the same type of half-space described previously with an attenuation of 0.3 dB/cm/MHz without any electronic noise added. In the first simulation, both the reference waveform and the backscattered waveforms were windowed with hamming windows with the same length *L*, as was done previously. Then, both

were windowed with rectangular windows of the same length. In the final simulation, the reference waveform was not windowed at all, and the backscattered waveforms were windowed by hamming windows. Although windowing functions other than hamming or rectangular could be used, the investigation of these functions is beyond the scope of this thesis. The results for all three of these simulations are shown in Figure 5.14. From these plots, it is clear that the best accuracy is achieved when the reference waveform and backscattered waveforms are windowed with the same hamming window function. However, windowing only the backscattered waveforms with a hamming window and the reference waveform with a rectangular window gives comparable performance. The worst performance is obtained using a rectangular window to gate both waveforms.

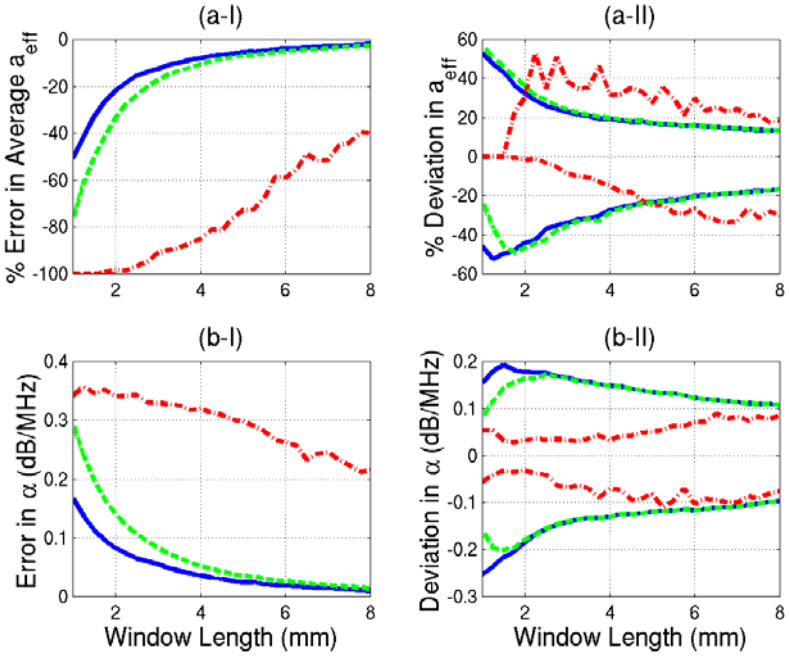

Figure 5.14: A comparison between different windowing functions; ▬ reference and backscattered waveforms windowed with same hamming window, ▬ ▪ ▬ reference and backscattered waveforms windowed with same rectangular window, and ▬ ▬ reference waveform not windowed and backscattered waveform windowed with hamming window. In the simulations, the half-space had an attenuation of 0.3 dB/cm/MHz and no electronic noise was added to the backscattered waveforms. Plots (a) compare the scatterer size estimates and plots (b) compare the total attenuation estimates. Plots (I) show the errors in the mean value for the estimates and plots (II) show the total deviation about the mean estimated values.

Using the same length hamming window to gate both the reference and backscattered waveforms provides some compensation for the blurring effects of the window on the spectrum. However, the compensation does not include the k_o^4 term that is later applied to the reference

spectrum from the plate. Therefore, to improve the performance of the algorithm at smaller window lengths other compensation techniques need to be considered. One possibility would be to use a reference phantom instead of a rigid plane at the focus to obtain the reference spectrum [*Gerig et al.*, 2003] and then use the same hamming window on both. However, a reference phantom will increase the uncertainty of the estimation technique [*Gerig et al.*, 2003]. Furthermore, it is difficult to perform a comprehensive evaluation of the reference phantom technique due to the need to test materials with attenuation, scatterer type, and scatterer sizes differing from the reference phantom. Hence, the reference phantom technique was not evaluated at this time. Instead, an attempt was made to directly compensate for the windowing effects on the backscattered waveforms while still using a rigid plane placed at the focus as a reference.

It has been shown that windowing of the signals in the time domain is equivalent to a convolution of the power spectra given by [*Wear*, 2002]

$$\mathrm{E}\left[\left|V_{refl}\right|^2\right]_{windowed} \propto \mathrm{E}\left[\left|V_{refl}\right|^2\right]_{ideal} * \left|G_{win}(f)\right|^2, \tag{5.8}$$

where $G_{win}(f)$ is the Fourier transform of the windowing function. Also, if the windowing function and expected backscattered spectra can be reasonably described by Gaussian distributions given by

$$\begin{aligned} \mathrm{E}\left[\left|V_{refl}\right|^2\right]_{ideal} &\propto \mathrm{e}^{-\frac{(f-f_o)^2}{2\sigma_\omega^2}} \\ \left|G_{win}(f)\right|^2 &\propto \mathrm{e}^{-\frac{f^2}{2\sigma_g^2}}, \end{aligned} \tag{5.9}$$

then the windowed backscattered spectrum is approximately given by [*Wear*, 2002]

$$\mathrm{E}\left[\left|V_{refl}\right|^2\right]_{windowed} \propto \mathrm{e}^{-\frac{(f-f_o)^2}{2\left(\sigma_\omega^2+\sigma_g^2\right)}}. \tag{5.10}$$

Hence, the windowing will increase the bandwidth of the backscattered waveform leading to an underestimate of the scatterer size for smaller window lengths as was observed in the above results. Furthermore, the broadening, as described in this manner, can be compensated by multiplying the windowed spectrum by

$$G_{corr} = \mathrm{e}^{-\frac{(f-f_o)^2\sigma_g^2}{2\left(\sigma_\omega^2+\sigma_g^2\right)\sigma_\omega^2}}. \tag{5.11}$$

This correction for windowing was tested by a simulation assuming a half-space as described above with an attenuation of 0.3 dB/cm/MHz. The backscattered spectrum from 25 independent RF echoes windowed with hamming windows without any additive electronic noise were averaged together in the normal frequency domain yielding $\mathrm{E}\left[\left|V_{refl}\right|^2\right]_{windowed}$. The resulting average spectrum was then fit by a Gaussian distribution in the log domain, as is discussed in Chapter 4, to obtain values for f_o and $\left(\sigma_\omega^2 + \sigma_g^2\right)$. The Fourier transform of the hamming window was also calculated and fit by a Gaussian distribution in the normal frequency domain to obtain the value of σ_g^2. G_{corr} was then calculated and applied from these parameters. Because the effects of windowing on the backscattered spectrum were directly compensated, no windowing was applied to the reference spectrum from the rigid plane. The results of this simulation are shown with the results using a hamming window for both the reference and backscattered signals from before in Figure 5.15. Clearly, the correction term allows for accurate estimates of total attenuation and scatterer size down to window lengths of 1 mm. However, the precision of the estimates continues to degrade for the smaller window lengths.

Instead of correcting for the windowing after averaging the spectra from the 25 independent RF echoes, it is also possible to apply the correction to each RF echo individually before averaging. Therefore, the simulation was repeated with G_{corr} being found and applied before the spectra were averaged using the updated frequency range described in the next section. The results for finding and applying G_{corr} both before and after averaging are shown in Figure 5.16. From Figure 5.16, it is clear that the blurring effect of windowing should be corrected after the spectra have been averaged together in the frequency domain.

5.2.3 Updating frequency range used for fit

In the earlier simulations, the frequency range used by the algorithm was dictated by Equation (4.9). However, this definition of the frequency range is not robust and depends heavily on the sampling rate used to acquire the data. Therefore, before the algorithms can be reliably implemented by other investigators, a better definition of the usable frequency range needs to be obtained. Because the whole purpose in selecting the frequency range is to exclude spectral regions dominated by system noise, a suitable alternative would be to select only those frequencies whose signal levels were reasonably larger than the noise floor. Hence, a more

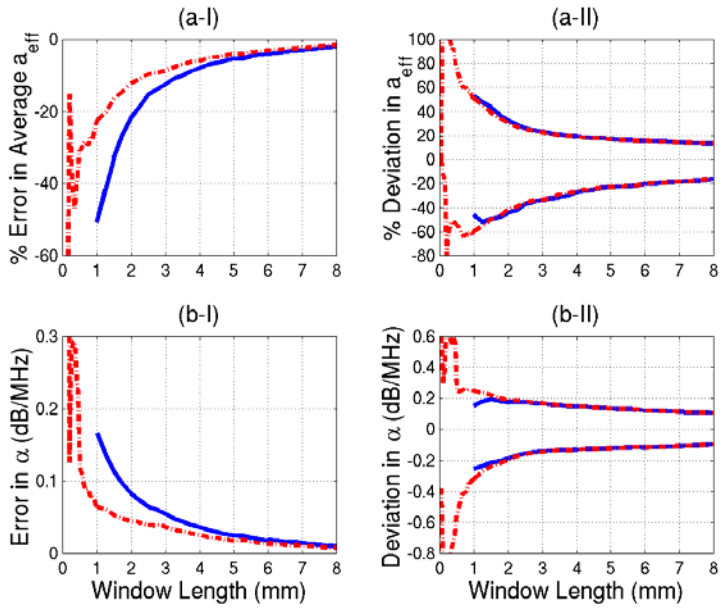

Figure 5.15: A comparison between (I) the mean values for the estimates (accuracy) and (II) the deviations about the mean values (precision) for both (a) scatterer size and (b) total attenuation when using the same hamming window to window the reference and backscattered waveforms, ——, and using G_{corr} to correct for the effects of windowing, -·-·-. In the simulations, the half-space had an attenuation of 0.3 dB/cm/MHz and no electronic noise was added to the backscattered waveforms.

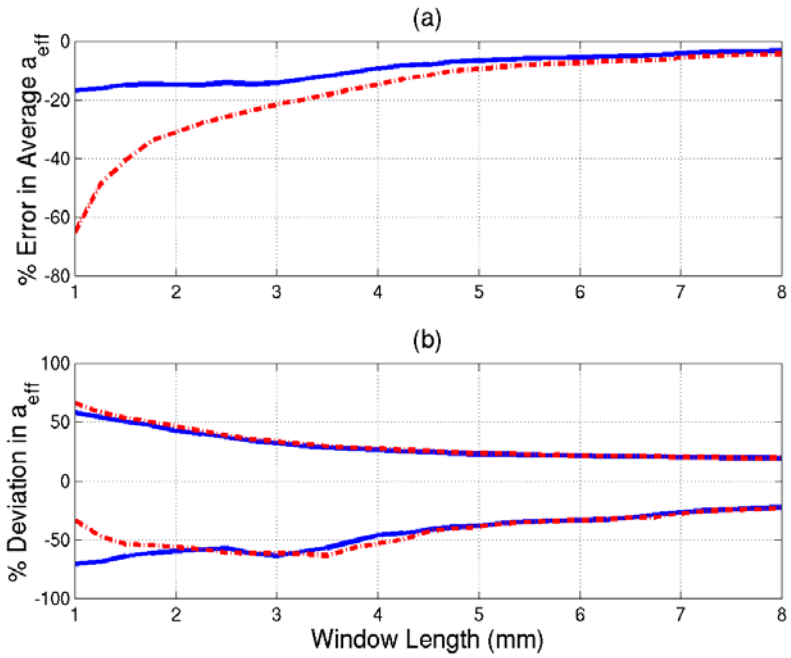

Figure 5.16: A comparison between (a) the mean values for the scatterer size estimates (accuracy) and (b) the deviations in scatterer size about the mean values (precision) when finding and correcting for windowing using G_{corr} after averaging the spectra, ——, and on each spectra individually before averaging, -·-·-. In the simulations, the half-space had an attenuation of 0.3 dB/cm/MHz and no electronic noise was added to the backscattered waveforms.

generalized selection criteria for the proper frequency range to perform the estimates is given by the set of all frequencies corresponding to signal levels greater than

$$N_{Floor} = \max\left(\left[\begin{array}{cc} N_{dB} & \text{mean}\left(10\log\left(\dfrac{P_{scat}\left(f_{N-200}:f_N\right)}{\max\limits_{\forall f}\left(\left\{P_{scat}\left(f\right)\right\}_{\substack{Gaussian\\ fit}}\right)}\right)\right)+6\end{array}\right]\right), \tag{5.12}$$

where N_{dB} sets a limit on the frequency range in the absence of any electronic noise and f_N refers to the largest positive frequency after taking the DFT of the sampled waveforms. In the simulations, N_{dB} was set to either –20 dB or –30 dB, and the signal was sufficiently oversampled so that at least the last 200 frequency samples would correspond to the additive white electronic system noise. Hence, Equation (5.10) only uses signal frequencies greater than 6 dB above the noise floor.

$\mathrm{E_N}\left[\left|N(f)\right|^2\right]$ used in compensating for the electronic noise by dividing the received spectrum by the term $\left(1+\mathrm{E_N}\left[\left|\mathrm{N(f)}\right|^2\right]\Big/\mathrm{V_{scat}(f)}\Big|_{\mathrm{measured}}\right)$ might also be obtainable from $P_{scat}\left(f_{N-200}:f_N\right)$, removing the need to record the noise in the absence of a transmitted signal. In order to test this possibility, the simulation results given in Figure 5.13 were repeated using $\mathrm{E_N}\left[\left|N(f)\right|^2\right]$ obtained from both a reference noise signal as well as by averaging the last 200 values of P_{scat}. In addition, the convolution effects of windowing were compensated and the frequency range used in the minimization was given by Equation (5.12) with N_{dB} set to –20 dB. The results for both methods of obtaining $\mathrm{E_N}\left[\left|N(f)\right|^2\right]$ are shown in Figure 5.17 along with the results obtained without any electronic noise compensation. Both methods for obtaining an estimate for $\mathrm{E_N}\left[\left|N(f)\right|^2\right]$ perform about the same and give significant improvement in the accuracy compared to when the electronic noise is not compensated validating the hypothesis from Section 5.2.1. Due to the comparable performance, in the future $\mathrm{E_N}\left[\left|N(f)\right|^2\right]$ will be found from the last 200 values of P_{scat}, removing the need to record the noise in the absence of a transmitted signal.

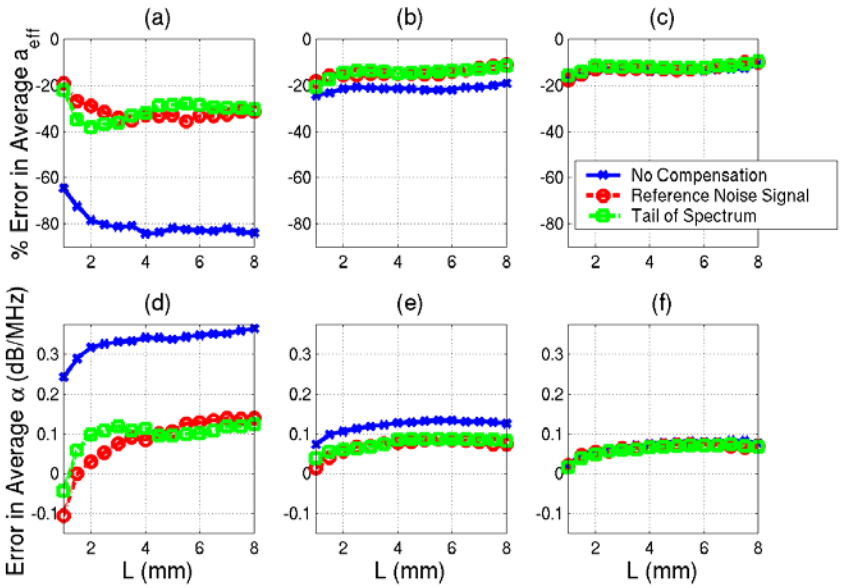

Figure 5.17: Comparison of errors in scatterer size estimates for *SNR*s of (a) 9 dB, (b) 23 dB, and (c) 36 dB as well as attenuation estimates for *SNR*s of (d) 9 dB, (e) 23 dB, and (f) 36 dB without noise compensation and with different methods for estimating $E_N\left[\left|N(f)\right|^2\right]$ for a half-space with an attenuation of 0.05 dB/cm/MHz.

5.3 Chapter Summary

In this chapter, the performance of the basic Spectral Fit algorithm for determining the total attenuation and scatterer size simultaneously was assessed. The performance of the basic Spectral Fit algorithm was reasonable for attenuations less than 0.8 dB/cm/MHz, *SNR*s for 23 dB to 28 dB, and window lengths of 8 mm. The limiting factor of the performance was a lack of precision with increasing noise, decreasing window length, and increasing attenuation. Hence, Chapters 6 and 7 will focus on improving the precision of the estimator. Also, several modifications to the basic Spectral Fit algorithm were evaluated. First, a comparison of averaging the pulse echo waveforms in the log spectral domain was compared to the averaging of the waveforms in the traditional spectral domain and found to be slightly less precise. Likewise, the electronic noise compensation term was evaluated and found to yield a significant improvement on the accuracy of the estimates. Then, the blurring effects of windowing were corrected assuming that the backscattered spectrum could be reasonably approximated as a Gaussian distribution. Lastly, a new criterion for selecting the frequency range over which the Spectral Fit algorithm would perform the required minimization was explained.